

Temporal evolution of cracking in prestressed concrete studied using a continuous-damage approach

Junying Rao, Chi Chen, and Tongyan Pan

- A study of the effect of time-dependent cracking behavior of prestressed concrete is presented.
- A continuous-damage approach is applied to a tool for modeling cracking behavior in prestress concrete related to prestress losses caused by steel stress relaxation, concrete creep, and concrete shrinkage.
- The tool developed using a three-dimensional finite-element method model will allow better understanding of the behavior of these members.

Concrete is a common construction material, owing to the low costs of its materials, production, and maintenance. Concrete is known to have high compressive strength but low tensile strength, which necessitates the use of strengthening steel in the tension zones of concrete structures. Modern concrete structures can be strengthened either passively with mild-steel reinforcing bars, which is known as reinforced concrete, or actively with high-strength prestressing tendons (or alloy bars), which is known as prestressed concrete. Although the uses of prestressed concrete members aim to minimize tensile cracking of concrete, reinforced concrete members often work with cracks allowed in tension zones. Moreover, newer construction practices tend to use prestressed concrete members more economically by including reinforcing bars in tension areas to control concrete cracking, producing partially prestressed concrete members.

Prestressed concrete and partially prestressed concrete members are more popular than reinforced concrete for building long-span and small-cross-section structures. With concrete cracking well controlled, partially prestressed concrete members have the advantage of significantly enhanced load-carrying capacity compared with prestressed concrete members. Concrete cracking not only reduces sectional capacity but also causes many durability problems, such as steel reinforcement corrosion and accelerated chemical degradation of the concrete matrix, in structures that cannot easily be fixed. Currently, design of concrete structures is governed by codes that mandate conservative strength-reduction factors.

PCI Journal (ISSN 0887-9672) V. 64, No. 6, November–December 2019.

PCI Journal is published bimonthly by the Precast/Prestressed Concrete Institute, 200 W. Adams St., Suite 2100, Chicago, IL 60606.

Copyright © 2019, Precast/Prestressed Concrete Institute. The Precast/Prestressed Concrete Institute is not responsible for statements made by authors of papers in *PCI Journal*. Original manuscripts and discussion on published papers are accepted on review in accordance with the Precast/Prestressed Concrete Institute's peer-review process. No payment is offered.

Considering the ubiquitous occurrence of microcracking or cracking in concrete structures, more research is needed to study the mechanism and extent of cracking and to develop more-effective strategies to control concrete cracking. This is particularly necessary for prestressed concrete and partially prestressed concrete structures that are more sensitive to concrete cracking than reinforced concrete structures.

In prestressed concrete and partially prestressed concrete structures, before service load is applied, prestressed steel tendons exert compressive stress in the concrete around the tendons while causing tensile stress in the opposite side of the structures. Prestressed concrete and partially prestressed concrete structures can be made by pretensioning or post-tensioning the tendons, depending on whether the tendons are stressed before or after concrete is cast. Due to the prestressing techniques used or the rheological properties of the concrete and steel materials, part of the applied prestressing force in the tendons will be lost and unavailable for use. This is known as prestress loss, and it can be categorized into instantaneous losses and time-dependent losses. While instantaneous losses, such as elastic shortening of the concrete and friction loss, can be effectively controlled by prestress compensation when the tendons are stressed, the three major types of time-dependent losses (relaxation of steel, creep of concrete, and shrinkage of concrete) occur over time. A time-dependent prestress loss has two concurrent but opposite effects on the concrete of a structure. First, the prestress loss reduces the prestress in steel, thereby reducing the stress, strain, and cracking tendency of concrete. Alternatively, as concrete creeps and/or shrinks, the concrete material yields extra deformation (in addition to instantaneous elastic deformation) in the direction of prestress, enhancing the strain level in concrete and causing further concrete cracking.¹

Mechanistic-based analysis of the cracking process in the concrete matrix is a complex process characterized by non-linear elasticity, small-deformation plasticity, or quasi-brittleness, depending on the extent of cracking and discontinuity inside the concrete matrix.²⁻⁴ For researchers and designers to effectively monitor prestress and predict the remaining service lives of prestressed concrete and partially prestressed concrete structures, the authors have developed a tool that can accurately depict the process of time-dependent prestress losses as well as clearly display the initiation and propagation of concrete cracks at any point in time. Substantial though inadequate research has been conducted to study the prestress losses and evolution of cracks in concrete. Pioneering understanding of concrete creep behavior can be found in works by Bažant,⁵⁻⁸ in which a large number of formulas of creep were proposed for concrete under different conditions. Some of the proposed formulas have been simplified and adopted in the current design codes. Concrete shrinkage is a process involving factors of ambient relative humidity, temperature, used admixtures, and the geometry of concrete structures. Ayano and Wittmann⁹ formulated a shrinkage coefficient of cement-based material in terms of relative humidity and time.

The moisture loss in the study was measured using sliced solid specimens. Sant et al.¹⁰ studied the impact of shrinkage-reducing admixtures. Based on continuous damage theory, a smeared crack model for concrete was developed by Ngo and Scordelis¹¹ and Rashid.¹² Chen and Mahadevan¹³ used local relative crack density to describe the evolution of concrete cracking based on continuous damage theory. Menin et al.¹⁴ applied the continuous damage theory to reinforced concrete and found that the results of smeared cracks are consistent with experimental observations.

Time-dependent prestress losses

Within this paper, time-dependent prestress losses for prestressed concrete are reviewed, specifically as they relate to steel stress relaxation, concrete creep, and concrete shrinkage. Steel stress relaxation, concrete creep, and concrete shrinkage have been widely recognized to be the three primary causes of time-dependent prestress losses of prestressed concrete. The following section first quantifies the prestress loss by each cause, which will be used later for determining total prestress losses and incurred concrete cracking.

Steel stress relaxation

Steel stress relaxation, a major contributing factor of prestress loss in prestressed concrete and partially prestressed concrete, refers to the continuous decreasing of prestressing force originally applied in steel tendons. Steel stress relaxation stems from the rearrangement of the metallic atoms in steel along the direction of the externally applied prestressing force. Because the applied prestress stress often exceeds 70% of the yield strength of steel, prestressed tendons continue relaxing in concrete, leading to significant prestress loss. Steel stress relaxation in tendons is analogous to the creepage behavior of general solid materials and depends on the type of steel used and environmental factors such as temperature. Improper estimation of prestress loss due to steel relaxation in tendons may result in serious design problems. Trevino and Ghali¹⁵ proposed a formula to describe tendon relaxation, which is adopted in the *PCI Design Handbook: Precast and Prestressed Concrete*.¹⁶ For commonly used low-relaxation tendons, Eq. (1) determines the prestress loss due to steel stress relaxation $\Delta\sigma_{pR}$ ¹

$$\Delta\sigma_{pR} = \sigma'_{pi} \left(\frac{\log t_2 - \log t_1}{45} \right) \left(\frac{\sigma'_{pi}}{\sigma_y} - 0.55 \right) \quad (1)$$

where

- σ'_{pi} = initially applied prestress in steel
- t_2 = end of the time interval for determining prestress loss
- t_1 = beginning of the time interval for determining prestress loss
- σ_y = yield strength of steel tendon

Concrete creep

Creep is a behavior involving continuously increasing strain in solid materials under sustained load. Numerous experimental data have demonstrated that creep in concrete material is a time-dependent rheological process that depends on temperature, concrete type, and stress level. In prestressed concrete and partially prestressed concrete structures, creep occurs mainly in hydrated cement paste, owing to the rheology of calcium silicate hydrates, and plays an important role in concrete cracking. Pioneering efforts in studying concrete creep effects were made by Bažant⁵ and his group as summarized in a compliance function. The compliance function can be expanded with Dirichlet series per Eq. (2) and has been applied in works of many other researchers.¹⁷ At each time step, an updating stress was used for replacing the stress of the previous step to calculate creep strain. The compliance function was then multiplied by stress to obtain creep strain.

$$J(t, \sigma) = \frac{1}{E_0(1 - e^{-\alpha\sigma})} + \sum (A_i + B_i\sigma^{-G_i}) \left(1 - e^{-S_i(t-\sigma)}\right) + D(e^{S_3\sigma} - e^{S_3t}) \quad (2)$$

where

$J(t, \sigma)$ = compliance function

E_0 = initial elastic modulus

α = experimentally measured fitting parameter

σ = stress

A_i = experimentally measured fitting parameter

B_i = experimentally measured fitting parameter

G_i = experimentally measured fitting parameter

S_i = experimentally measured fitting parameter

t = time

D = experimentally measured fitting parameter

Because creep strain is a long-term effect that causes concrete deformation under sustained load (such as prestressing force), the prestress in tendons can be reduced by the creep strain of concrete due to the strain compatibility at the steel-concrete interface. Although Eq. (2) can readily describe creep behavior in concrete, in engineering practice simpler formulas are commonly used. Nawy provides a simple formula as Eq. (3) to calculate creep loss in term of stress,¹ which depends on time and load magnitude.

$$\Delta\sigma_{pCR} = C_t \frac{E_{ps}}{E_c} \sigma_{cs} \quad (3)$$

$$\varepsilon_{CR} = C_t \varepsilon_{EL} \quad (4)$$

$$C_t = \frac{t^{0.6}}{10 + t^{0.6}} C_u \quad (5)$$

where

$\Delta\sigma_{pCR}$ = prestress loss due to concrete creep

C_t = creep coefficient as a function of time

E_{ps} = elastic modulus of prestress steel tendon or wires

E_c = elastic modulus of concrete

σ_{cs} = stress in concrete at the location of the centroid of steel tendon

ε_{CR} = concrete creep strain

ε_{EL} = linear elastic strain

C_u = ultimate creep coefficient

To obtain the creep coefficient, Branson¹⁸ proposed a model per Eq. (5) that was based on rheological theory and adopted by PCI. The ultimate creep coefficient C_u varies from 2 to 4 according to experimental data. PCI suggests that the values of the ultimate creep coefficient center around 2.35. Concrete cracking by concrete creep is primarily due to compression creep; however, the continuous damage tool used in this study captures the maximal principal strain in each element as the cracking criteria, whether or not it is caused macroscopically by compression creep or tensile creep.

Concrete shrinkage

Shrinkage is an inherent property of concrete related to the moisture loss in curing or cured concrete. Shrinkage of concrete can be classified differently into plastic shrinkage, drying shrinkage, autogenous shrinkage, and carbonation shrinkage.¹⁹ The autogenous and carbonation types of shrinkage usually are not considered for most engineering applications. The plastic shrinkage occurs as fresh concrete sets in the mold, while drying shrinkage is a long process in hardened concrete that depends on factors such as average ambient temperature, moisture, and curing conditions. Both phenomena were reviewed. Experimental data indicate that the average ultimate shrinkage strain of typical concrete is 780×10^{-6} ,¹ regardless of curing and service conditions. For typical prestressed concrete, most shrinkage loss takes place within the first year of the structure life. Branson¹⁸ proposed several equations for shrinkage strain (Eq. [6] and [7]), where the ultimate shrinkage strain of concrete $\varepsilon_{SH,u}$ is equal to 780×10^{-6} , according to Nawy.¹ Equations (6) and (7) apply to the moist-curing conditions and steam-curing conditions, respectively. Equation (8) gives the PCI-specified prestress loss by shrinkage strain.

$$\varepsilon_{SH} = \frac{t}{35+t} \varepsilon_{SH,u} \quad (6)$$

$$\varepsilon_{SH} = \frac{t}{55+t} \varepsilon_{SH,u} \quad (7)$$

$$\Delta\sigma_{pSH} = \varepsilon_{SH} \times E_{ps} \quad (8)$$

where

ε_{SH} = concrete shrinkage strain

$\Delta\sigma_{pSH}$ = prestress loss due to concrete shrinkage

Continuous damage of concrete

Mathematical modeling of time-dependent prestress loss and evolution of concrete cracks is rather challenging. The highly nonlinear equations generally require a numerical solution for these problems formulated as a continuous or discrete crack model. De Borst et al.²⁰ compared and explained the applications of the continuous and discrete crack models implemented using the finite element method (FEM). Explicitly modeling the time-dependent prestress loss and evolution of discrete concrete cracks by FEM is challenging because the FEM model must keep remeshing the discontinuous surface and generating the mesh of a singularity geometry, which is time consuming. To simplify the process of crack development, the continuous damage theory, in which cracks are nucleated into vicinal elements, has commonly been used. Vicinal elements of an element in this study refer to the neighborhood elements that are located not far from the element. Also, the mechanical properties, such as moduli and Poisson ratio, can be reduced by retention factors when using the continuous crack approach.

In this study, the constitutive relation of plasticity was implemented to calculate the strain and stress needed to formulate the continuous damage of concrete as a solid continuum. In the plasticity theory of solid mechanics, stress increments associated with plastic strain and elastic strain are linked by a fourth-order elasticity modulus tensor and a plasticity modulus tensor.¹⁹ In this study, the total strain in prestressed concrete was decomposed into linear elastic strain ε_{EL} , plastic strain ε_{PL} , shrinkage strain ε_{SH} , and creep strain ε_{CR} (Eq. [9]). The Kronecker delta δ is involved to calculate the shrinkage strain and creep strain as a component of the total strain, as both shrinkage and creep can only result in volumetric deformation rather than deviatoric strain. The shrinkage in aggregate and the creep in steel are significantly small compared with creep and shrinkage in mortar. Therefore, the aggregate phase and steel phase of concrete structures generally only involve linear elastic ε_{EL} and plastic strain ε_{PL} .

$$(\varepsilon_{total})_{ij} = (\varepsilon_{EL})_{ij} + (\varepsilon_{PL})_{ij} + (\varepsilon_{SH})_{ij} \delta_{ij} + (\varepsilon_{CR})_{ij} \delta_{ij} \quad (9)$$

where

δ_{ij} = element of Kronecker delta matrix at the i^{th} row and the j^{th} column

Concrete is a quasi-brittle material that tolerates small plastic deformation before cracking. There are two general methods to model concrete cracks: the discrete method and the extended method. Based on classical fracture mechanics, the discrete method involves modeling cracks as a stress singularity with fracture energy release in a crack-tip zone. To track the crack propagation and locate crack tips in consecutive steps, it is necessary to remesh the local domain of the FEM model to adjust geometry variety at the crack tips and calculate the released fracture energy. Pan and Wang²¹ used a cohesive surface approach to simulate the evolution of concrete cracks. A J-integral was used by Pan and Wang to track the propagation of cracks and calculate the crack distance close to the crack tips. In classical FEM, however, it is difficult to apply the discrete method to remeshing crack-tip elements. In addition, the numerical computation is unstable and does not easily converge at crack tips because of the discontinuity of displacement and singularity of stress. The development of the extended FEM (XFEM), with the partition of unity, offers a new approach to overcome stress singularity and displacement discontinuity.²² For microcracking of concrete, however, it is still challenging to simulate the development of a large number of cracks with the XFEM.¹³

Similarly to material hardening and softening, the elastic modulus tensor was calculated from the stress and strain tensor; that is, the modulus tensor matrix depended on the principal stress and strain and its orientation.²⁵ Alternatively, the rotating-crack model hypothesis is that the crack direction is orthogonal to the principal tensile strain, which is introduced a transformation matrix T (Eq. [10]) to update stress-strain direction and elastic modulus from the principal direction to the global direction.²⁵⁻²⁷ In Eq. (10), l , m , and n denote the directions of principal stresses, where the subscripts 1, 2, and 3 denote the cosine angle between the principal stress direction and the x, y, or z axis in the global coordinate system. The multidirectional fixed-crack model allows for an intermediary performance between the single-crack model and the rotating-crack model, such that multiple cracks can develop from the same point.^{14,27}

$$T = \begin{bmatrix} l_1^2 & m_1^2 & n_1^2 & 2l_1m_1 & 2n_1l_1 & 2m_1n_1 \\ l_2^2 & m_2^2 & n_2^2 & 2l_2m_2 & 2n_2l_2 & 2m_2n_2 \\ l_3^2 & m_3^2 & n_3^2 & 2l_3m_3 & 2n_3l_3 & 2m_3n_3 \\ l_1l_2 & m_1m_2 & n_1n_2 & l_1m_2 + l_2m_1 & l_1n_2 + l_2n_1 & m_1n_2 + m_2n_1 \\ l_1l_3 & m_1m_3 & n_1n_3 & l_1m_3 + l_3m_1 & l_1n_3 + l_3n_1 & m_1n_3 + m_3n_1 \\ l_2l_3 & m_2m_3 & n_2n_3 & l_2m_3 + l_3m_2 & l_2n_3 + l_3n_2 & m_2n_3 + m_3n_2 \end{bmatrix} \quad (10)$$

In rotating and multidirectional fixed-crack models, the deteriorated stiffness matrix D^s in the global coordinate system is calculated from the elastic modulus matrix in the crack plane D^{cr} by Eq. (11). However, the numerical resolution does not

easily converge and it is necessary to introduce two factors, μ and β , to simplify and improve the FEM calculation (Eq. [12]).^{28,29} The factors μ and β are known as the coefficient of normal reduction and shear retention factor, respectively.³⁰ The coefficient of normal reduction depends on the stress-strain curve of concrete obtained in experiment data, accounting for material hardening and softening properties. The shear retention factor varies from 0 to 1.

$$D^s = \begin{matrix} \underbrace{D^s}_{6 \times 6} = \underbrace{T^{-1}}_{6 \times 6} \underbrace{D^{cr}}_{6 \times 6} \underbrace{T}_{6 \times 6} & (11) \\ \left[\begin{array}{cccccc} \mu E & 0 & 0 & 0 & 0 & 0 \\ 0 & \mu E & 0 & 0 & 0 & 0 \\ 0 & 0 & \mu E & 0 & 0 & 0 \\ 0 & 0 & 0 & \beta G & 0 & 0 \\ 0 & 0 & 0 & 0 & \beta G & 0 \\ 0 & 0 & 0 & 0 & 0 & \beta G \end{array} \right] & (12) \end{matrix}$$

where

E = elastic modulus

G = shear modulus

The total strain obtained from Eq. (9) was then linked to the stress status by a fourth-order stiffness tensor per Eq. (13). The stiffness tensor is symmetric, which indicates that the tensor

can be reduced to a second-order tensor and expressed as a 6×6 matrix in the 3-D space. Once the total strain exceeds the limit strain of the material, the deteriorated stiffness matrix D^s derived from Eq. (11) replaces the original stiffness matrix.

$$\sigma_{ij} = D_{ijkl} (\epsilon_{total})_{kl} \quad (13)$$

where

σ_{ij} = stress status

D_{ijkl} = fourth order stiffness tensor

ϵ_{total} = total strain

FEM model of prestressed concrete slab

The time-dependent cracking damage process of a pretensioned concrete slab was modeled in this study. Simple supports are applied on the two end sides of the slab, and the boundaries of the other two sides are left open. The volume-to-surface ratio equals 0.13 for the slab. A 1.31×1.31 ft (0.4×0.4 m) portion of the slab was chosen for detailed micromechanical analysis (Fig. 1). The overall dimensions of the concrete slab are 24×5 ft (7.3×1.5 m)

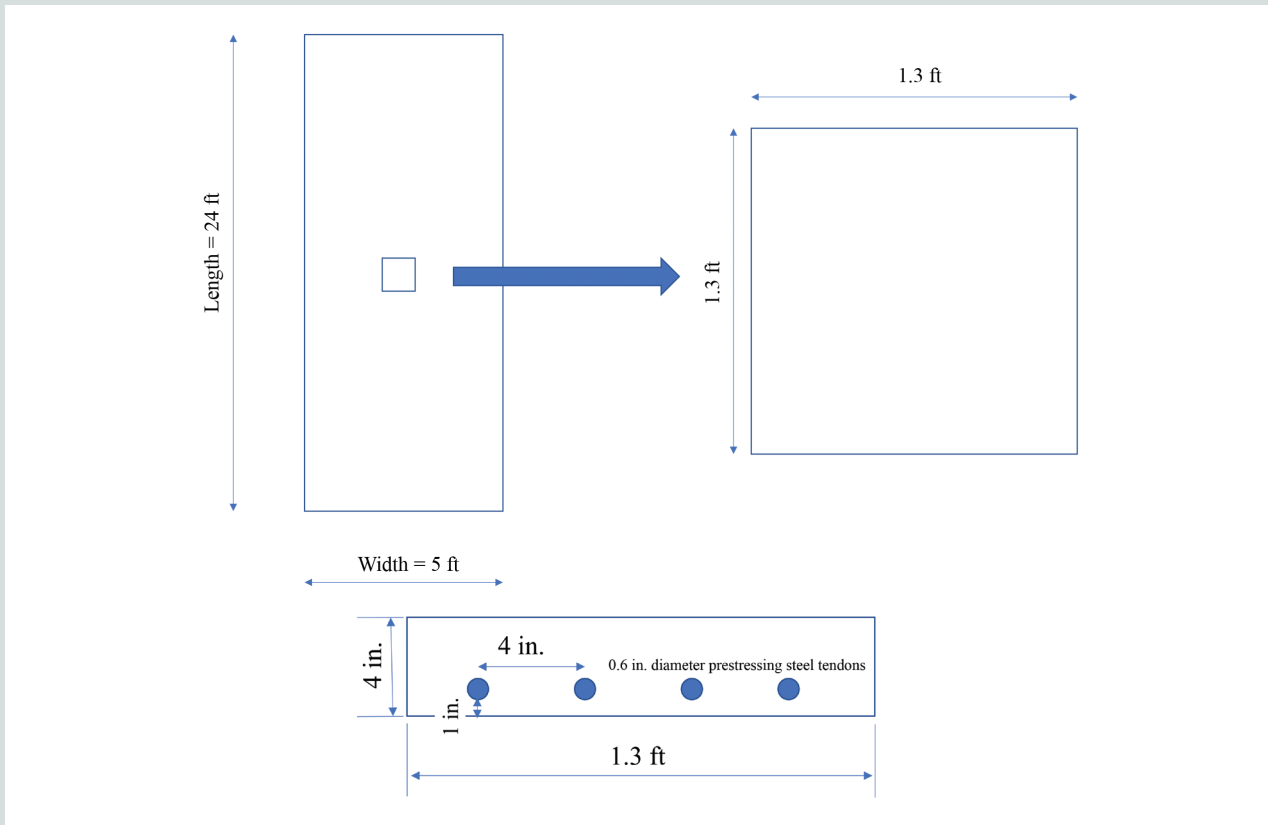


Figure 1. Dimensions of global and local prestressed concrete slabs for finite element method models. Note: 1 in. = 25.4 mm; 1 ft = 0.305 m.

with a 1 in. (25.4 mm) concrete cover. Moderate-strength prestressing tendons, each made of seven-wire compacted strands of Grade 270 ($\sigma_{pu} = 270,000$ psi [1860 MPa]) steel, with a 0.6 in. (15.2 mm) nominal diameter were selected as the prestressing steel (consistent with ASTM A722³¹). The seven-wire strands were made of a low-relaxation steel, which is applicable to Eq. (1). The top and bottom extreme fiber stresses of the concrete slab due to the prestressing force were determined by Eq. (14) and (15). After instantaneous prestress losses, the initial prestressing stress $\sigma_{pi} = 0.6\sigma_{pu}$ was obtained. The strand was spaced at a 4 in. (101.6 mm) center-to-center distance. A high compressive strength concrete with $f'_c = 6000$ psi (41,370 kPa) was used in the slab model. Many researchers report that most concrete shrinkage and creep occurs in hydrated cement paste due to the characteristics of hydration products.^{1,6} Creep is a complicated process that depends on the stress level, temperature, water-cement ratio, and relative humidity, for which empirical constants can be expressed by a compliance function.⁷ To simplify the calculation in this study, the creep strain in concrete was obtained using Eq. (4) provided by Nawy,¹ which is a function of time and strain level. Shrinkage strain of concrete was obtained using Eq. (6) and (7). The elastic modulus of concrete was calculated based on the strength of concrete per Eq. (16).

$$\sigma^t = -\frac{F_i}{A_c} + \frac{F_i e y_t}{I_g} \quad (14)$$

$$\sigma^b = -\frac{F_i}{A_c} + \frac{F_i e y_b}{I_g} \quad (15)$$

$$E_c = 57,000 \sqrt{f'_c} \quad (16)$$

where

σ^t = top fiber stress of cross section

F_i = initial prestressing force

A_c = cross-sectional area

e = eccentricity

y_t = distance from neutral axis to top edge of cross section

I_g = moment of inertia

σ^b = bottom fiber stress of cross section

y_b = distance from neutral axis to bottom edge of cross section

A small physical sample of the prestressed concrete slab was subjected to an X-ray computed tomography (CT) scanner, and a series of two-dimensional (2-D) CT images that reflect the inner structure of concrete were obtained. A 3-D FEM model associated with the CT images of the prestressed concrete slab sample was developed by the authors to conduct micromechanical analysis.³² **Figure 2** shows the 3-D FEM micromechanical model with three different phases (mortar, aggregate, and steel) reconstructed from scanned 2-D CT images of the prestressed concrete slab sample. Perfect bonding was assumed between the steel and concrete in the model. As discussed, the shrinkage of the concrete slab only occurs in the mortar phase, and Eq. (6) was used for this moist-cured slab. The elastic modulus of concrete was calculated to be 4.5×10^6 psi (31,000 MPa) per Eq. (16). The elastic modulus for the Grade 270

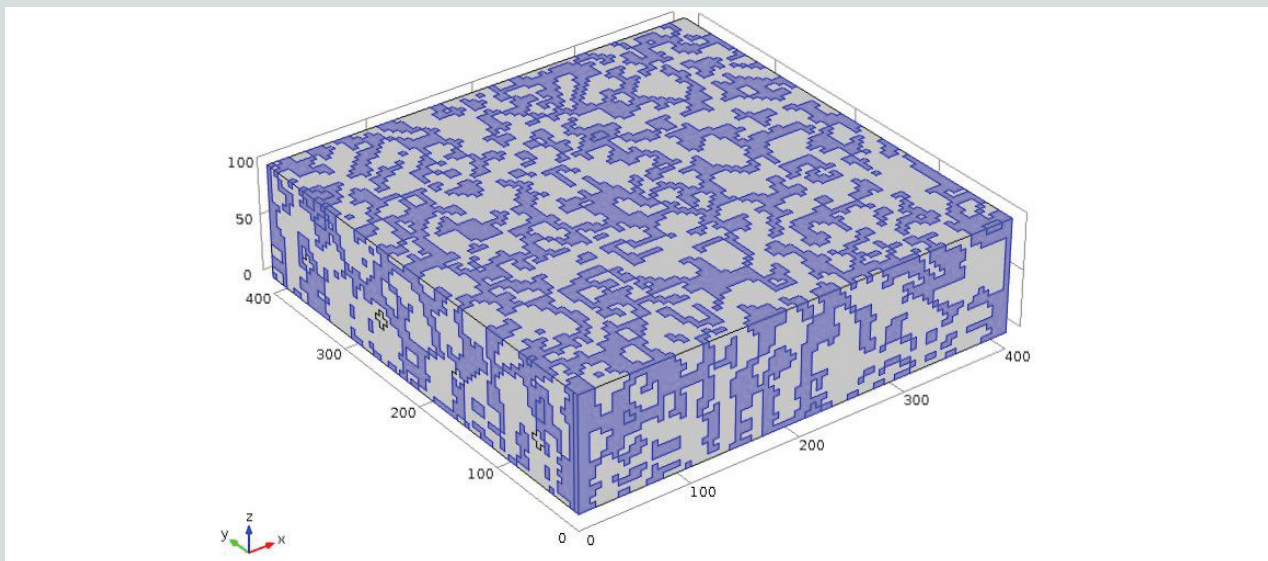


Figure 2. Microscopic structure of prestressed concrete slab for detailed micromechanical analysis. Note: All dimensions are in millimeters. 1 mm = 0.0394 in.

(1860 MPa) steel tendon was 29×10^6 psi (200,000 MPa), and the elastic modulus of the aggregate phase was 10×10^6 psi (69,000 MPa). The Poisson ratio was assumed to be 0.20 for these solid materials.

Twenty CT images (80×80 pixels each) were used to create the 3-D FEM micromechanical model of the prestressed concrete slab sample. Each 2-D pixel was reconstructed to a 3-D voxel of $0.2 \times 0.2 \times 0.2$ in. ($5 \times 5 \times 5$ mm) in dimension, representing a hexahedral FEM element. The modeled prestressed concrete slab had dimensions of $16 \times 16 \times 4$ in. ($400 \times 400 \times 100$ mm) (Fig. 2). Continuous damage theory was then implemented to analyze the 3-D FEM micromechanical model. This model contained 128,000 elements and 137,781 nodes. Each node had three degrees of freedom: u_x, u_y, u_z . A transient solver was adopted to solve for the cracking behavior of the prestressed concrete slab. To implement the finite element analysis with the constitutive relation per Eq. (13), the weak form of the equilibrium equation was required for FEM simulation (Eq. [17]). More details about derivation of the weak form of constitutive equation can be found in the authors' previous studies.³²

$$\int_{\Omega} B_e^T D_{n-1} B_e d\Omega \Delta u_n = P^{ext} - P_{n-1}^{int} \quad (17)$$

$$= \int_{\Gamma} N_e p d\Gamma - \int_{\Omega} B_e \sigma_{n-1} d\Omega = R_{n-1}$$

where

B_e = the first derivative of N_e function

N_e = shape function of eight-node element

Ω = integration domain

u_n = displacement variable

P^{ext} = external force vector

P^{int} = internal force vector

Γ = integration boundary

p = load vector

R_{n-1} = residual vector at the $n-1$ step

Initial and boundary conditions for analysis using FEM

Initial prestress and prestress losses in tendons

Based on the assumed initial prestress in tendons f_{pi} equal to 60% of the ultimate strength of the tendon steel and the thickness (cross-sectional area) of the tendon steel, an initial prestressing force F_i of 45,800 lb (204,000 N) was obtained and applied to the tendons. The prestress losses due to concrete creep and concrete shrinkage were calculated per Eq. (3) and (8). The prestress loss due to tendon steel relaxation was calculated per Eq. (1). The value of σ_{cs} for creep loss calculation was 1750 psi (12,000 kPa) for Eq. (3) based on the self-weight of the slab only. **Figure 3** shows the three different types of prestress loss for a one-year period. The shrinkage of concrete was the primary factor that affected prestress loss owing to the high surface area-to-volume ratio of the slab. Also, all three types of prestress loss evolved rapidly in the first 180 days and tended to level off at one year, meaning that most of the prestress loss occurred

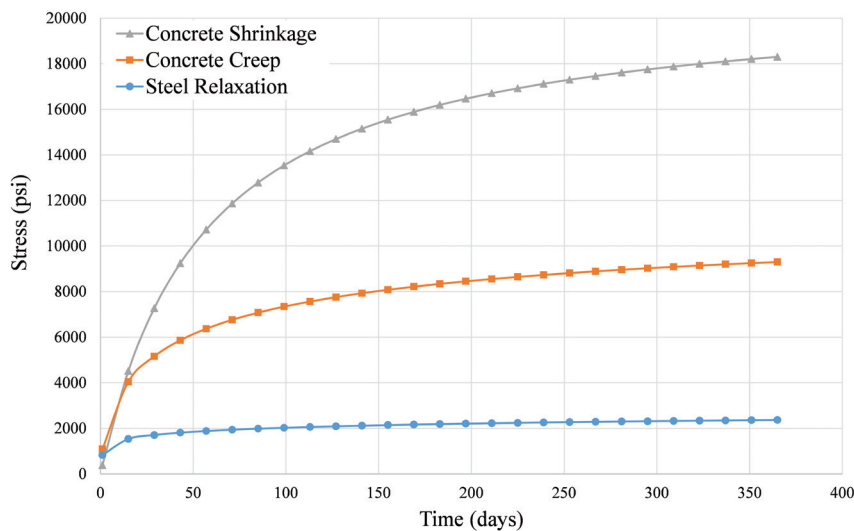


Figure 3. Different types of prestress loss with time. Note: 1 psi = 6.895 kPa.

within the first half year and was almost complete in the first year after prestress transfer. This is consistent with general field observations in the prestressed concrete industry. Figure 3 shows that the total prestress loss due to concrete creep, shrinkage, and steel relaxation was about 26,500 psi (182,700 kPa), or 16% of the initial prestress, after 180 days, which is in the normal range. These initial values were then used for FEM simulation.

Boundary conditions

Figure A.1 shows the location and the displacement boundary conditions of the 3-D FEM micromechanical model (for appendix figures, go to pci.org/2019Nov-Appx-Pan). On the left-hand side of the 3-D FEM micromechanical model, a symmetric boundary was applied, meaning that no rotation is allowed on this side. In other words, this side was only subjected to moment and horizontal load. On the right side of the slab, a vertical hinged-support boundary was applied, meaning that only rotation was allowed and no vertical displacement was permitted. Under such assumed boundary conditions, the shear stress was zero on the symmetric boundary, which is consistent with basic structure mechanics.

For the force/stress boundary conditions of the 3-D FEM micromechanical model, on the right side, the moment M_D (43,000 lb-in. [5 kN-m]) was transmitted from the remaining part of the prestressed concrete slab. The stress by M_D on this side was determined from the initial prestress f_{pt} in the tendon. The self-weight W_D of the slab caused shear stress and moment in the concrete (Fig. A.2). The moment on the 3-D FEM micromechanical model can be broken down into three parts: moment caused by prestress tendon with nonzero eccentricity,

moment transmitted from remaining concrete of the slab, and self-weight-caused moment (Fig. A.3).

Parameters for 3-D FEM micromechanical model

A shear retention factor β (Eq. [12]) value of 0.2 was adopted according to a prior study.²³ The coefficient of normal reduction μ is a function of ultimate strain; that is, the post-peak behavior and softening process of concrete are needed to determine the relationship between the ultimate strain and normal reduction. To simplify the FEM computation, a normal reduction factor value of 0.5 was adopted for crushed concrete and a value of 0.1 was adopted for open cracks.^{29,33} To minimize the convergence problem during numerical simulation, the Poisson ratio of the deteriorated concrete matrix was set with a small starting value.

Validation of boundary conditions

The specified boundary conditions for the 3-D FEM micromechanical model of the concrete slab needed to be validated before detailed analysis using FEM. Two simple FEM models, termed local and global, where concrete is assumed to be homogeneous, were developed to validate the displacement and the mechanical boundary conditions. Figure 4 shows the vertical displacement u_z of the global prestressed concrete slab at the initial stage ($t = 0$). Simple supports were applied on the two end sides of the slab, while the boundaries of the other two sides were left open. The maximum displacement (camber) occurred at the center of the slab, with a value of 2.03 in. (51.6 mm). For the local FEM model shown in Fig. 4, the displacement boundary condition is specified in Fig. A.1 and

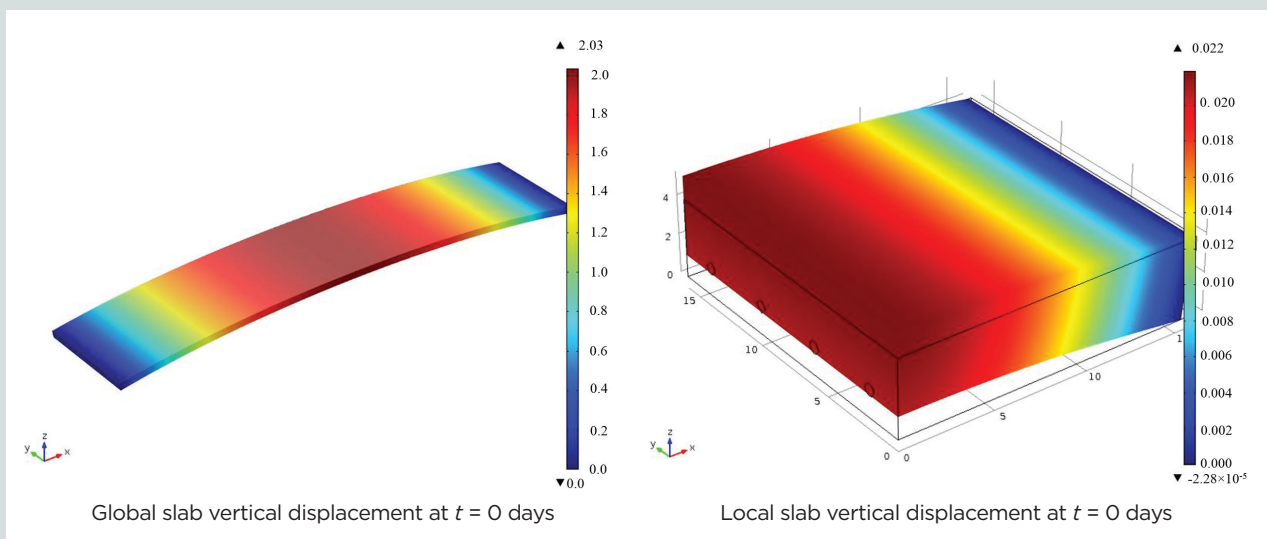


Figure 4. Vertical displacements predicted for homogeneous prestressed concrete slab according to global (left) and local (right) finite element method models. Note: All dimensions are in inches. t = time. 1 in. = 25.4 mm.

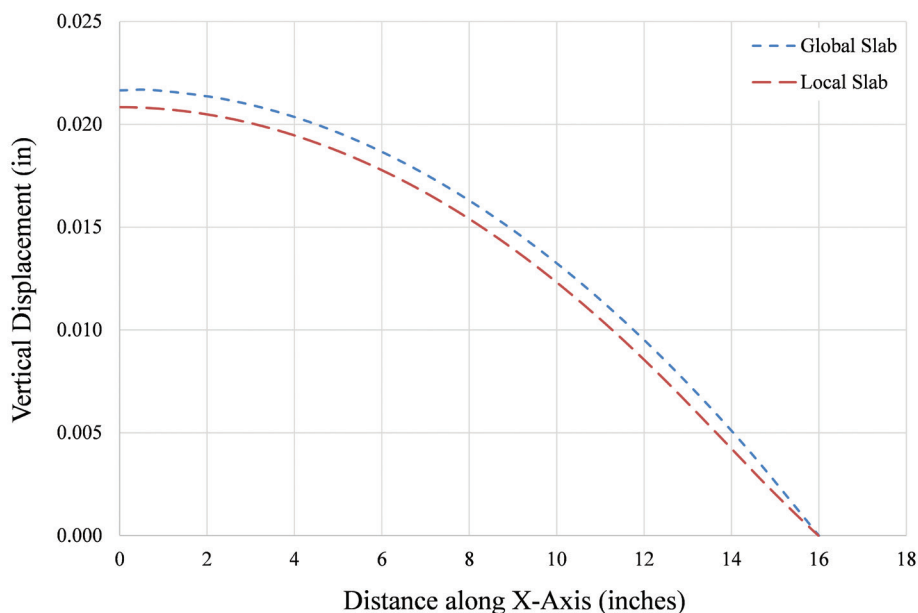


Figure 5. Comparison of vertical displacement predictions for prestressed concrete slab according to global and local slab finite element method models. Note: 1 in. = 25.4 mm.

the force boundary condition is given in Fig. A.3, where the moment transmitted from the remaining part of the concrete was calculated to be 43,000 lb-in. (5 kN-m). Figure 4 displays the vertical displacement u_z of the local FEM model. The left side of this piece of concrete slab represents the centerline of the global prestressed concrete slab. The camber difference between the left and right sides was about 0.02 in. (0.5 mm).

To more effectively validate the boundary conditions of the two simple FEM models, the difference between the vertical displacements of the left and right sides of the local FEM model were plotted in **Fig. 5**, with one curve predicted by the global FEM model and the other predicted by the local FEM model. Figure 5 shows that the vertical displacements between the two sides were close to each other (within 3%), as predicted by the global and local FEM models. This indicates that the boundary conditions specified for the local FEM model were appropriate. Such boundary conditions for displacements and forces were then used in subsequent finite element analysis of the 3-D FEM micromechanical model.

Results and discussion

The validated boundary conditions were then applied to the 3-D FEM micromechanical model with the concrete microstructure reconstructed from X-ray CT images (Fig. 2). This 3-D FEM micromechanical model was developed to more accurately determine localized stress and strain concentrations where excessive displacement, stress, or strain may have occurred, causing concrete cracking. The concrete slab

was subjected to prestressing force from steel tendons, the self-weight of the slab, and the three time-dependent prestress loss processes: tendon steel relaxation, concrete creep, and concrete shrinkage. This slab is simply supported at two ends, which is a statically determinate structure in which thermal expansion is allowed and temperature-caused stress is negligible. Most of the total time-dependent prestress loss occurs in the first half year after prestress transference (Fig. 3); thus, in many cases prestress loss can be assumed to be complete within the first year. From this standpoint, the prestress losses were modeled for 180 days in this study, starting from the moment of prestress transference. Figure 3 further shows that all three types of time-dependent prestress loss progressed rapidly within the first month of prestress transference and that over 80% of the total time-dependent prestress loss occurred within the first 180 days.

Figure 6 shows the vertical deflection of the micromechanical prestressed concrete slab under prestressing force and self-weight and experiencing the three time-dependent prestress loss processes at the moments of 0 days, 30 days, 60 days, and 180 days. The prestressing force had its maximum value at the initial stage before prestress loss. As expected, the vertical deflection of the prestressed concrete slab had a maximum value of 0.022 in. (0.56 mm) at 0 days, which matched the result predicted by the two simple FEM models shown in Fig. 5. This observation shows that the 3-D FEM micromechanical model was developed correctly. Over time, the vertical displacement of the prestressed concrete slab progressed at slower rates as more prestress loss occurred. Figure 6 shows

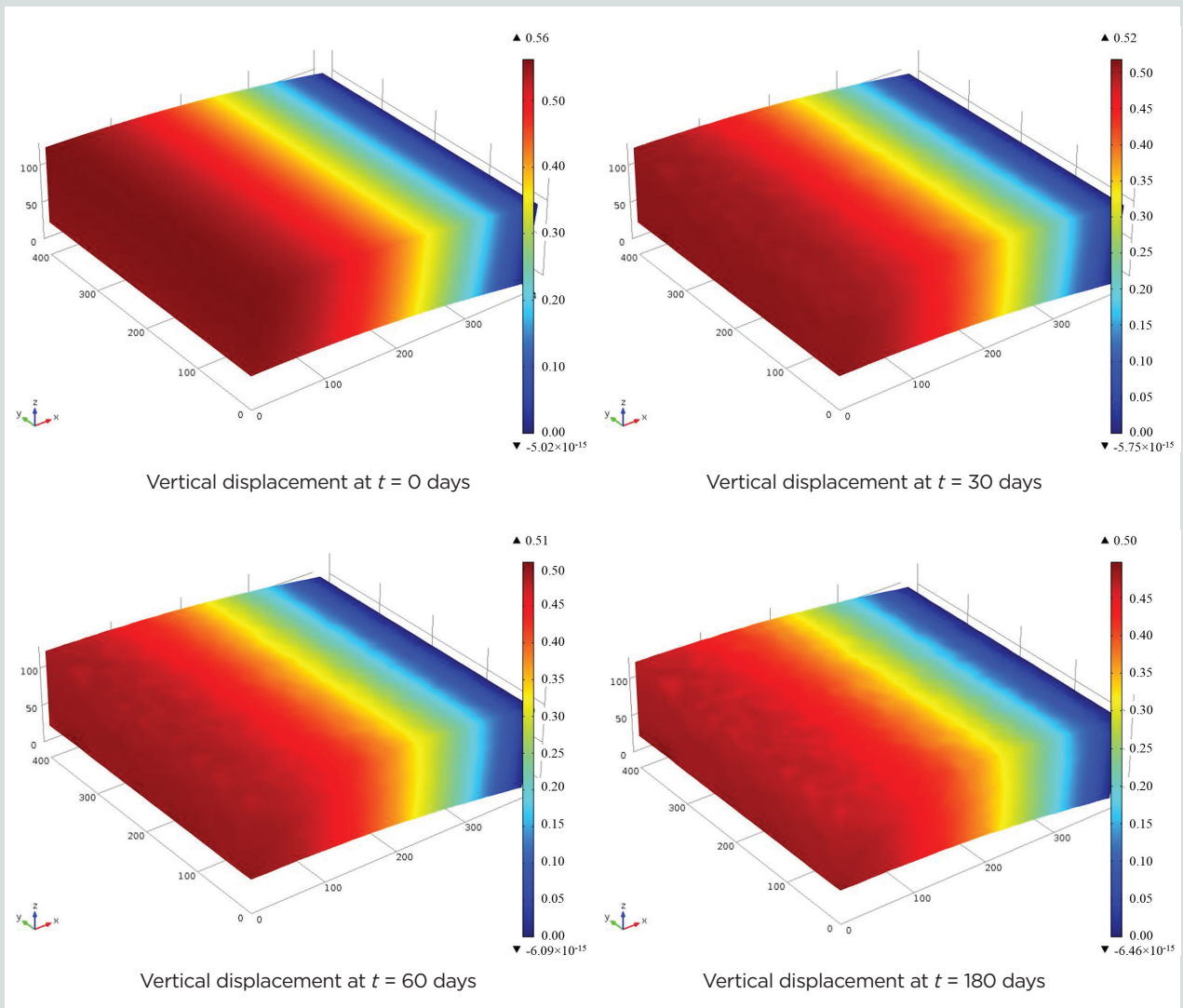


Figure 6. Vertical displacement of prestressed concrete slab according to 3-D finite element method micromechanical model at 0 days, 30 days, 60 days, and 180 days. Note: All dimensions are in inches. t = time. 1 mm = 0.0394 in.

that the value of vertical displacement decreased most significantly within the first 30 days. This is because most of the prestress loss happened within the first 30 days. In addition, in Fig. 6 the vertical deflection of the prestressed concrete slab appears to be distributed nonuniformly inside the concrete slab because the mortar and aggregate phases in concrete have different mechanical properties. This differentiates the results from the simple FEM models shown in Fig. 5.

To more clearly examine the variation of vertical deflection in the prestressed concrete slab, the top edge of the left side of the slab was selected for a detailed analysis. **Figure 7** shows the vertical displacement magnitudes of the selected edge at different time moments. At the beginning, the vertical displacement of the prestressed concrete slab demonstrated a smooth curve. As time progressed, the curve became more nonuniformly distributed in the slab due to the three types

of prestress loss. Such nonuniform distribution in deformation might indicate localized stress and strain concentrations where concrete cracking could occur. **Figure 7** shows that the vertical displacement of the left side of the concrete slab decreased by about 20% from 0 to 180 days, which shows the significant effect of prestress loss on the behavior of a prestressed concrete structure.

For the prestressed concrete slab modeled in this study, the primary strain and stress occur in the direction along the tendons, that is, the x-axis direction shown in Fig. 4 and 6. **Figure 8** shows the evolution of the primary strain, which is the normal strain along the x-axis direction, with time. In this study, positive values refer to tension and negative values indicate compression. Prestressing force from steel tendons applied eccentrically can cause moment on the cross section (Fig. A.3). **Figure 8** shows that in the beginning the slab was subjected to

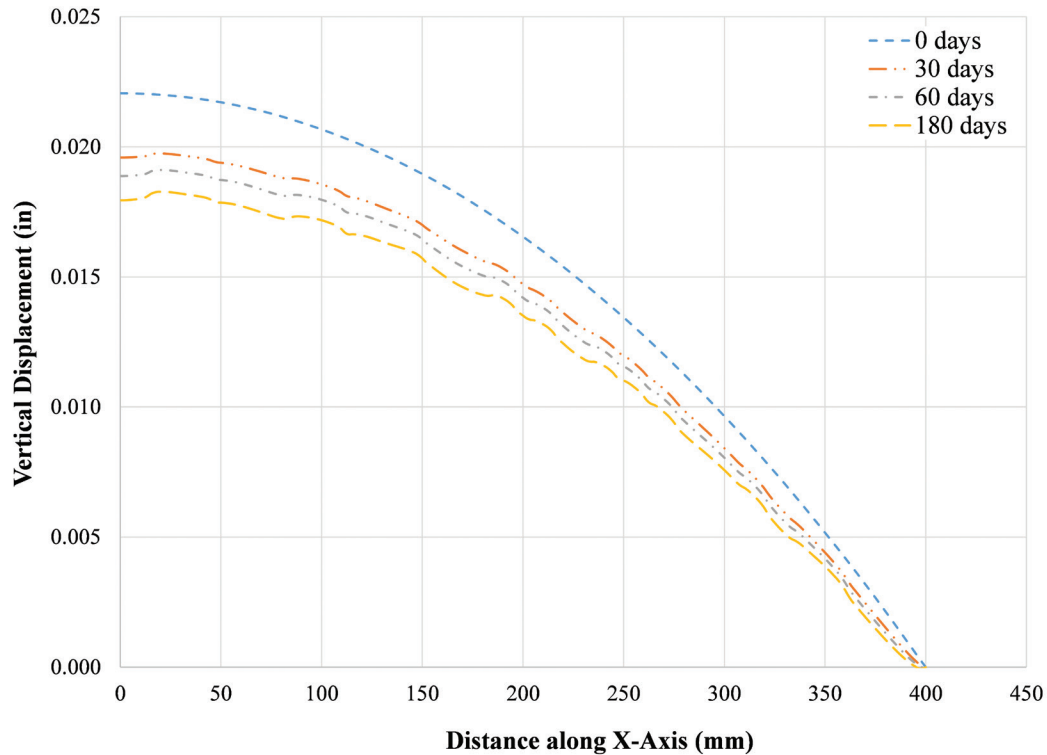


Figure 7. Vertical displacement along selected edge prestressed concrete slab at different times. Note: 1 in. = 25.4 mm. 1 mm = 0.0394 in.

tensile strain in its upper cross section and compressive strain in the lower cross section. As time progressed, prestress loss due to steel relaxation in the tendons took effect by decreasing the magnitude of prestressing-force-caused moment, leading to reduced strain in the concrete. It is noteworthy that the difference in stress and strain is small between aggregate and paste.

The shrinkage and creep of concrete occurred primarily in the hardened mortar phase. Figure 8 shows that over time the normal strain in the concrete slab tended to become compressive strain, even on the top of the slab. This is because the shrinkage and creep of concrete aggravated the compressive strain as the concrete material (mainly mortar) yielded under the prestressing force. Figure 8 shows that the compressive strain caused by shrinkage and creep of concrete was more significant and larger than the tensile strain resulting from the eccentric prestressing force. After 30 days, the mortar phase of concrete was under tension while the aggregate phase was under compression, leading to concentrated internal strain and stress in the prestressed concrete slab. On the right side of the slab, the localized high deformation and strain in concrete around the tendon–concrete interface was significantly higher than the deformation and strain at other locations of the slab owing to the St. Venant’s effect, meaning that the stress, strain, and deformation are significantly higher in the close vicinity of where load is applied than the location away from the loaded area. In design prac-

tices, such concentrated strain should be controlled to prevent catastrophic failure at the prestress transference stage.

The principal strain in the concrete was then used to trace and evaluate the development of cracks in the prestressed concrete slab based on the continuous damage theory. The strain status of a point in a concrete domain can be expressed by a 3×3 symmetric matrix in the 3-D spatial coordinate system. To determine the magnitude and direction of the principal strain at a point in the domain, the eigenvalue and eigenvector of the matrix need to be determined. Equations (18) and (19) show the eigenproblem for finding the principal stress or strain for the concrete domain, where l , m , and n , and denote the direction of the three principal strains. Three eigenvectors should be obtained and substituted into Eq. (13) to obtain the principal stress. In Eq. (19), I_1 , I_2 , and I_3 represent the first, second, and third invariants of strain, respectively.

According to the continuous damage theory, concrete cracking occurs when the principal tensile strain of an element in the concrete domain exceeds a predetermined strain limit; similarly, concrete crushes when the principal compressive strain of an element in the concrete domain exceeds a predetermined strain limit. The concrete stiffness can be deteriorated by either the tensile cracking or compressive crushing. If the principal strain of a concrete element possesses a value

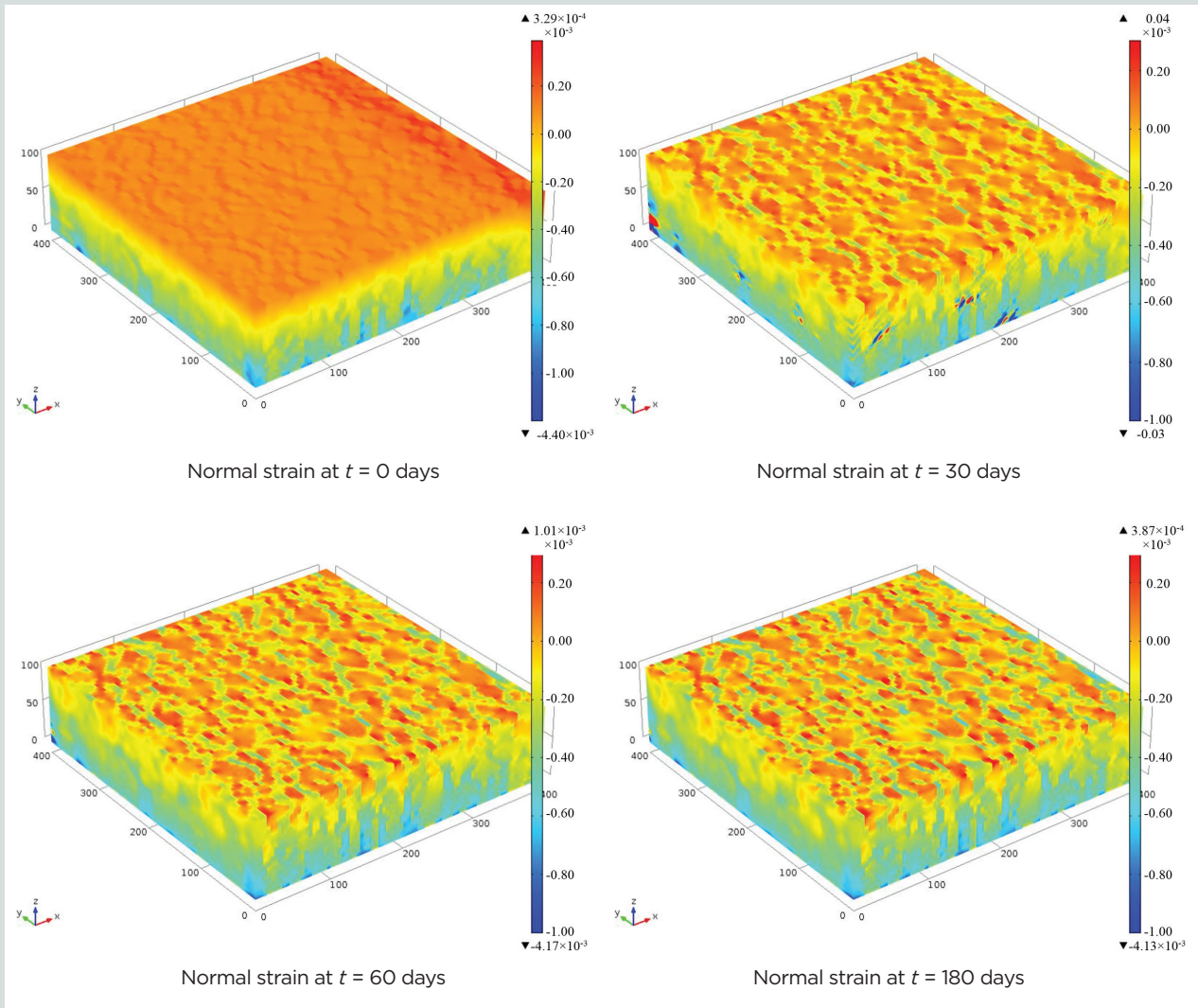


Figure 8. Normal strain along x axis of prestressed concrete slab at 0 days, 30 days, 60 days, and 180 days. Note: All dimensions are in millimeters. t = time. 1 mm = 0.0394 in.

between the tensile and compressive limits, the element is characterized as uncracked or uncrushed.

$$\begin{bmatrix} m \\ n \\ l \end{bmatrix} \begin{bmatrix} \varepsilon_{11} & \varepsilon_{12} & \varepsilon_{13} \\ \varepsilon_{21} & \varepsilon_{22} & \varepsilon_{23} \\ \varepsilon_{31} & \varepsilon_{32} & \varepsilon_{33} \end{bmatrix} = \begin{bmatrix} m \\ n \\ l \end{bmatrix} \varepsilon \quad (18)$$

$$\varepsilon^3 + I_1 \varepsilon^2 + I_2 \varepsilon + I_3 = 0 \quad (19)$$

Figure 9 shows the evolution of concrete cracking based on the continuous damage theory, that is, the principal strain criterion, from 0 to 180 days. The 0 value in Fig. 9 represents the stiffness-degraded elements, and 1 represents the stiffness-undegraded elements (original elements). Figure 9 shows that no cracks occurred at the time of prestress transference ($t = 0$). Although the prestress loss in tendons tends to reduce the strain in concrete in the x-axis direction, the shrinkage

and creep of concrete always yield unrecoverable strain in the direction of prestressing force, which will contribute to the total strain level and cause cracking or crushing of concrete. This complex process of concrete damage under the cumulative effects of prestressing force and prestress losses can only be properly studied using a 3-D FEM micromechanical model as developed in this study.

At 30 days, a few cracks occurred near the center of the prestressed concrete slab (Fig. 9). These cracks at the slab center then closed and new cracks started to appear on the surface of the slab after 60 days. Most of these cracks were caused by the compressive strain from concrete shrinkage and creep. Whether the crack is micro or macro after 180 days depends on the density of the elements that are shown as cracked in Figure 9, from which it can be seen that although most cracks are sporadic, some do merge to appear as major cracks. In this study, the drying shrinkage played a more important role in concrete cracking due to the high surface area-to-volume ratio of the

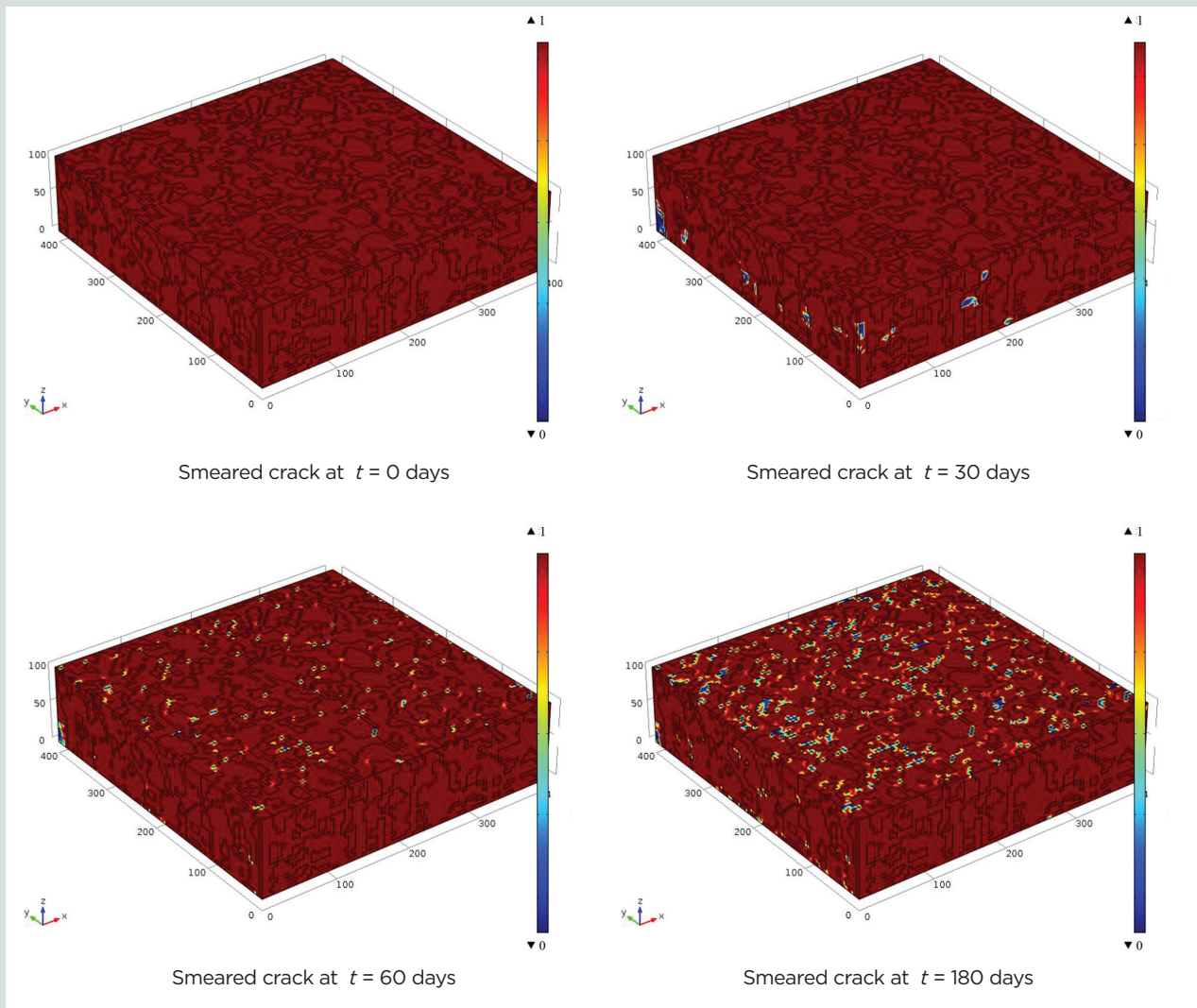


Figure 9. Accumulated continuous damage of prestressed concrete at 0 days, 30 days, 60 days, and 180 days. Note: All dimensions are in millimeters. t = time. 1 mm = 0.0394 in.

slab. Moisture in concrete can evaporate from the slab surface, where the shrinkage strain is proportional to moisture loss. Also, compared to the macro tension field, the micro or local tension strain and stress, because of the difference properties of paste and aggregate, are significantly higher, which contributes a lot to the cracking of concrete. Drying shrinkage generally only causes microcracks in concrete.³⁴ It is noteworthy that there is difference between the prestress loss of pretensioned concrete versus post-tensioned concrete. In post-tensioned concrete, since there are additional non-time-dependent losses due to seating and friction and there is no transfer zone, the time-dependent cracking of concrete may be less severe owing to the smaller prestressing force in the tendon.

To further study the contribution of the time-dependent prestress losses to the cracking behavior of concrete, the individual effect of each type of prestress loss was evaluated separately. **Figure A.4** shows the evolution of concrete damage under the effect of tendon relaxation alone by holding the concrete creep

and shrinkage constant. No cracks occurred in the prestressed concrete slab during the 180-day period. Without concrete creep and shrinkage considered, the maximum strain appeared at the very beginning stage. Over time, the intensity of the principal strain decreased as the tendon steel relaxed.

Figure A.5 shows the evolution of concrete damage under the concrete creep effect alone by holding the steel relaxation and concrete shrinkage constant, which did not result in apparent concrete cracking. Equations (3) and (4) characterize the creep strain associated with stress level or linear elastic strain. The coefficient of creep strain is a factor that depends on time. Without concerning other types of prestress loss, the level of stress in concrete σ_{cs} is from the initial prestressing force applied to tendons at the initial stage. In this study, because the eccentricity of prestressing force was small, the level of stress in concrete σ_{cs} did not result in high stress to cause significant creepage of concrete. As a result, the total creep strain did not exceed the tensile or compressive limits for concrete cracking or crushing.

Figure A.6 displays the evolution of concrete damage by the effect of concrete shrinkage alone by holding the steel relaxation and concrete creep constant. A few cracks appeared near the center of the concrete slab at 30 and 60 days. At 180 days, many more cracks appeared on the slab surface as a result of significant moisture loss over time. Compared with the effects of tendon relaxation and concrete creepage, the prestress loss by concrete shrinkage played a more important role in concrete cracking. This observation is in agreement with the results shown in Fig. 3, where the shrinkage loss was more significant for the prestressed concrete slab. As such, attention should be given to the concrete shrinkage effect in the design and manufacture of prestressed concrete slabs. It is noteworthy that shrinkage of concrete has a typical range from 400 to 1000 microstrain relative to the assumed 780 microstrain in this paper; therefore in reality, the actual extent of concrete cracking may be significantly more severe than what is predicted in this manuscript since concrete shrinkage plays a more important role in the cracking damage of prestressed concrete slabs than steel stress relaxation and concrete creep. Considering the limited research done in numerically studying the time-dependent cracking of prestressed concrete,^{35–37} this work can be expected to improve the knowledge base of the subject.

Conclusion

This paper presents a 3-D FEM micromechanical model based on the continuous damage theory and a time-dependent analysis of the cracking behavior of prestressed concrete slab. Three major types of prestress loss (tendon steel relaxation, concrete shrinkage, and concrete creep) were formulated based on the current concrete design codes and modeled explicitly in the developed model. Based on constitutive equations of plasticity mechanics, stress in concrete was determined and updated at each time step to compute the principal strain used in the 3-D FEM micromechanical model based on continuous damage theory. Coefficients of the normal reduction factor and shear retention factor were induced to improve the efficiency of the FEM computation. A prestressed concrete slab was analyzed using the developed tool based on the 3-D reconstructed microstructure of concrete. Boundary conditions and initial values for the 3-D FEM micromechanical model were validated by two simplified FEM models. The total time-dependent prestress loss was found to be 16% of the initial prestress applied to the tendon. The displacement, principal strain, and cracking damage of the 3-D FEM micromechanical model were analyzed. The model outputs showed that prestress loss could significantly affect the cracking behavior of prestressed concrete. Stress concentration caused by prestress losses could cause concrete cracking even if the initial concrete stress from the tendon prestress was below the cracking and crushing limits of concrete. In addition, it was found that concrete shrinkage plays an important role in the cracking damage of prestressed concrete slabs because such slabs often have a high surface area-to-volume ratio. Results were verified by separately analyzing the effect of each time-dependent

prestress loss. This comprehensive study provides a useful tool, by means of a 3-D FEM micromechanical model, for evaluating the cracking behavior and cumulative damage of prestressed concrete structures.

References

1. Nawy, E. G. 2011. *Prestressed Concrete*. Upper Saddle River, NJ: Pearson Education.
2. Payan, C., V. Garnier, and J. Moysan. 2010. "Effect of Water Saturation and Porosity on the Nonlinear Elastic Response of Concrete." *Cement and Concrete Research* 40 (3): 473–476.
3. Chen, W. F. 2007. *Plasticity in Reinforced Concrete*. Fort Lauderdale, FL: J. Ross Publishing.
4. Shah, Surendra P., S. E. Swartz, and C. Ouyang. 1995. *Fracture Mechanics of Concrete: Applications of Fracture Mechanics to Concrete, Rock and Other Quasi-Brittle Materials*. New York, NY: John Wiley & Sons.
5. Bažant, Z. P. 1988. *Mathematical Modeling of Creep and Shrinkage of Concrete*. Z. P. Bažant, editor. New York, NY: Wiley.
6. Bažant, Z. P., and S. Prasannan. 1989. "Solidification Theory for Concrete Creep. I: Formulation." *Journal of Engineering Mechanics* 115 (8): 1691–1703.
7. Bažant, Z. P., A. B. Høgggaard, S. Baweja, and F. J. Ulm. 1997. "Microprestress-Solidification Theory for Concrete Creep. I: Aging and Drying Effects." *Journal of Engineering Mechanics* 123 (11): 1188–1194.
8. Bažant, Z. P., and S. Baweja. 2000. "Creep and Shrinkage Prediction Model for Analysis and Design of Concrete Structures: Model B3." *ACI Special Publications* 194: 1–84.
9. Ayano, T., and F. H. Wittmann. 2002. "Drying, Moisture Distribution, and Shrinkage of Cement-Based Materials." *Materials and Structures* 35 (3): 134–140.
10. Sant, G., A. Eberhardt, D. Bentz, and J. Weiss. 2010. "Influence of Shrinkage-Reducing Admixtures on Moisture Absorption in Cementitious Materials at Early Ages." *Journal of Materials in Civil Engineering* 22 (3): 277–286.
11. Ngo, D., and A. C. Scordelis. 1967. "Finite Element Analysis of Reinforced Concrete Beams." *Journal of the American Concrete Institute* 64 (3): 152–163.
12. Rashid, Y. R. 1968. "Ultimate Strength Analysis of Prestressed Concrete Pressure Vessels." *Nuclear Engineering and Design* 7 (4): 334–344.

13. Chen, D., and S. Mahadevan. 2007. "Cracking Analysis of Plain Concrete Under Coupled Heat Transfer and Moisture Transport Processes." *Journal of Structural Engineering* 133 (3): 400-410.
14. Menin, R. G., L. M. Trautwein, and T. N. Bittencourt. 2009. "Modelos de Fissuração Distribuída em Vigas de Concreto Armado Pelo Método dos Elementos Finitos." *RIEM-IBRACON Structures and Materials Journal* 2 (2): 166-182.
15. Treviño, J., and A. Ghali. 1985. "Relaxation of Steel in Prestressed Concrete." *PCI Journal* 83 (5): 82-94.
16. PCI Industry Handbook Committee. 2010. *PCI Design Handbook: Precast and Prestressed Concrete*. MNL-120. 7th ed. Chicago, IL: PCI.
17. Wu, Y., and R. Luna. 2001. "Numerical Implementation of Temperature and Creep in Mass Concrete." *Finite Elements in Analysis and Design* 37 (2): 97-106.
18. Branson, D. E. 1977. *Deformation of Concrete Structures*. New York City, NY: McGraw-Hill.
19. Ramamurthy, K., E. K. Nambiar, and G. I. S. Ranjani. 2009. "A Classification of Studies on Properties of Foam Concrete." *Cement and Concrete Composites* 31 (6): 388-396.
20. De Borst, R. 1987. "Smearred Cracking, Plasticity, Creep, and Thermal Loading—A Unified Approach." *Computer Methods in Applied Mechanics and Engineering* 62 (1): 89-110.
21. Pan, T., and L. Wang. 2011. "Finite-Element Analysis of Chemical Transport and Reinforcement Corrosion-Induced Cracking in Variably Saturated Heterogeneous Concrete." *Journal of Engineering Mechanics* 137 (5): 334-345.
22. Moës, N., J. Dolbow, and T. Belytschko. 1999. "A Finite Element Method for Crack Growth without Remeshing." *International Journal for Numerical Methods in Engineering* 46 (1): 131-150.
23. De Borst, R. 2002. "Fracture in Quasi-Brittle Materials: A Review of Continuum Damage-Based Approaches." *Engineering Fracture Mechanics* 69 (2): 95-112.
24. Bažant, Z. P., and B. H. Oh. 1983. "Crack Band Theory for Fracture of Concrete." *Materials and Structures* 16 (3): 155-177.
25. Petrangeli, M., and J. Ožbolt. 1996. "Smearred Crack Approaches—Material Modeling." *Journal of Engineering Mechanics* 122 (6): 545-554.
26. Vecchio, F. J., and A. DeRoo. 1995. "Smearred-Crack Modeling of Concrete Tension Splitting." *Journal of Engineering Mechanics* 121 (6): 702-708.
27. Rots, J. G. 1988. "Computational Modeling of Concrete Fracture." PhD diss., Delft University of Technology, the Netherlands.
28. Pimanmas, A., and K. Maekawa. 2001. "Multi-directional Fixed Crack Approach for Highly Anisotropic Shear Behavior in Precracked RC Members." *Doboku Gakkai Ronbunshu* 2001 (669): 293-307.
29. Dahmani, L., A. Khennane, and S. Kaci. 2009. "Modeling and Influence of Shear Retention Parameter on the Response of Reinforced Concrete Structural Elements." *Strength of Materials* 41 (4): 423-430.
30. De Borst, R., J. J. Remmers, A. Needleman, and M. A. Abellan. 2004. "Discrete vs Smearred Crack Models for Concrete Fracture: Bridging the Gap." *International Journal for Numerical and Analytical Methods in Geomechanics* 28 (7-8): 583-607.
31. ASTM Subcommittee A01.05. 2018. *Standard Specification for High-Strength Steel Bars for Prestressed Concrete*. ASTM A722/A722M-18. West Conshohocken, PA: ASTM International.
32. Pan, T., C. Chen, and Q. Yu. 2017. "Three-Dimensional Micromechanical Modeling of Concrete Degradation under Multiphysics Fields." *Composite Structures* 175 (1): 7-18.
33. Aquaro, D., G. Forasassi, and M. Marconi. "Ultimate Resistance of a Reinforced Concrete Foundation under Impulsive Loading." Paper H04-2 presented at the 17th International Conference on Structural Mechanics in Reactor Technology (SmiRT 17), August 17 -22, 2003, Prague, Czech Republic. <https://repository.lib.ncsu.edu/bitstream/handle/1840.20/27228/H04-2.pdf>.
34. Granger, L., J.-M. Torrenti, and P. Acker. 1997. "Thoughts About Drying Shrinkage: Experimental Results and Quantification of Structural Drying Creep." *Materials and Structures* 30: 588-598.
35. Jayaseelan, H., and B. W. Russell. 2019. "Reducing Cambers and Prestress Losses by Including Fully Tensioned Top Prestressing Strands and Mild Reinforcing Steel." *PCI Journal* 64 (3): 29-46.
36. Hariharan, V., G. Lucier, S. Rizkalla, P. Zia, G. Klein, and H. Gleich. 2019. "Behavior of Compact L-Shaped Spandrel Beams with Alternative Web Reinforcement." *PCI Journal* 64 (2): 39-54.
37. Sameer K. S. Pachalla, S. and Prakash, S. 2018. "Load Resistance and Failure Modes of Hollow-Core Slabs with

Notation

A_c	= cross-section area of concrete slab	l_2	= direction of principal stress at cosine angle between l and y axis
A_i	= experimentally measured fitting parameter	l_3	= direction of principal stress at cosine angle between l and z axis
B_e	= the first derivative of N_e function	m_1	= direction of principal stress at cosine angle between m and x axis
B_i	= experimentally measured fitting parameter	m_2	= direction of principal stress at cosine angle between m and y axis
C_t	= creep coefficient as a function of time	m_3	= direction of principal stress at cosine angle between m and z axis
C_u	= ultimate creep coefficient	n_1	= direction of principal stress at cosine angle between n and x axis
D	= experimentally measured fitting parameters	n_2	= direction of principal stress at cosine angle between n and y axis
D^{cr}	= elastic modulus matrix in the crack plane	n_3	= direction of principal stress at cosine angle between n and z axis
D_{ijkl}	= fourth order stiffness tensor	M_D	= moment for boundary conditions of 3-D FEM micromechanical model
D^s	= deteriorated stiffness matrix	N_e	= shape function of eight-node element
e	= eccentricity	p	= load vector
E	= elastic modulus	P^{ext}	= external force vector
E_c	= elastic modulus of concrete	P^{int}	= internal force vector
E_{ps}	= elastic modulus of prestress steel tendon or wires	R_{n-1}	= residual vector at the n-1 step
E_0	= initial elastic modulus	S_i	= experimentally measured fitting parameter
f'_c	= compressive strength of concrete	t	= time
f_{pi}	= initial prestress in tendon	t_1	= beginning of the time interval for determining prestress loss
F_i	= initial prestressing force	t_2	= end of the time interval for determining prestress loss
G	= shear modulus	T	= transformation matrix
G_i	= regression factor	u	= displacement variable
I_g	= moment of inertia of cross section	u_x	= displacement of 3-D FEM micromechanical model in x-axis direction
I_1	= first invariant of strain	u_y	= displacement of 3-D FEM micromechanical model in y-axis direction
I_2	= second invariant of strain	u_z	= vertical displacement of 3-D FEM micromechanical model
I_3	= third invariant of strain		
$J(t, \sigma)$	= compliance function		
l_1	= direction of principal stress at cosine angle between l and x axis		

W_D	= self-weight of 3-D FEM micromechanical model	ε_{SH}	= concrete shrinkage strain
y_b	= distance from neutral axis to bottom edge of slab	$\varepsilon_{SH,u}$	= ultimate shrinkage strain of concrete
y_t	= distance from neutral axis to top edge of slab	ε_{total}	= total strain
α	= experimentally measured fitting parameter	μ	= coefficient of normal reduction
β	= coefficient of shear retention factor	σ	= stress
Γ	= integration boundary	σ^b	= bottom fiber stress of concrete slab
δ	= Kronecker delta	σ_{cs}	= stress in concrete at the location of the centroid of steel tendon
δ_{ij}	= element of Kronecker delta matrix at the i^{th} row and the j^{th} column	σ_{ij}	= stress status
$\Delta\sigma_{pCR}$	= prestress loss due to concrete creep	σ_{pi}	= initial prestressing stress
$\Delta\sigma_{pR}$	= prestress loss due to steel stress relaxation	σ_{pu}	= ultimate strength of prestressing steel
$\Delta\sigma_{pSH}$	= prestress loss due to concrete shrinkage	σ^t	= top fiber stress of concrete slab
ε_{CR}	= concrete creep strain	σ_y	= yield strength of steel tendon
ε_{EL}	= linear elastic strain	Ω	= integration domain
ε_{PL}	= plastic strain		

About the authors



Junying Rao, PhD, is an associate professor in the College of Civil Engineering at Guizhou University in China.



Chi Chen, PhD, is a research assistant in the Department of Civil, Architectural and Environmental Engineering at the Illinois Institute of Technology in Chicago, Ill.



Tongyan Pan, PhD, PE, is this paper's corresponding author. He is an associate professor in the Department of Mathematics and Engineering at the University of Northwestern in St. Paul, Minn.

Abstract

The stringent control of cracking in prestressed concrete demands more research to investigate the mechanism and evolution of cracking in concrete under combined prestressing and loading conditions. For the first time, continuous damage theory is applied to quantitatively depict the time-dependent cracking behavior of prestressed concrete. A 3-D finite element method (FEM) micromechanical model based on the continuous damage theory was created for a prestressed concrete slab using a 3-D imaging-based approach developed for reconstructing a concrete microstructure. Three major time-dependent prestress losses—tendon relaxation, concrete shrinkage, and concrete creep—were determined explicitly using the developed 3-D FEM micromechanical model. Based on the determined deformation, principal strain, and level of cracking of the concrete slab, it was found that the time-dependent prestress losses significantly affect the cracking behavior of prestressed concrete. Stress growth resulting from prestress losses could cause chronic concrete cracking in service even if the initial prestress applied in concrete was well below its cracking limit. Of the three major types of prestress losses, concrete shrinkage plays a more critical role in causing continuous cracking in prestressed concrete. The 3-D FEM micromechanical model has the potential for wide adoption for designing prestressed concrete structures because, for example, concrete cracking can be more accurately predicted in design.

Keywords

Continuous damage, micromechanical modeling, time-dependent prestress loss.

Review policy

This paper was reviewed in accordance with the Precast/Prestressed Concrete Institute's peer-review process.

Reader comments

Please address any reader comments to *PCI Journal* editor-in-chief Emily Lorenz at elorenz@pci.org or Precast/Prestressed Concrete Institute, c/o *PCI Journal*, 200 W. Adams St., Suite 2100, Chicago, IL 60606. [P](#)